Pressure-induced structural phase transition in fullerides doped with rare-earth metals

Dam Hieu Chi,[1] Y. Iwasa,[1,2,3] K. Uehara,[1] T. Takenobu,[2,3] T. Ito,[1] T. Mitani,[1] E. Nishibori,[4] M. Takata,[4,5] M. Sakata,[4] Y. Ohishi,[5] K. Kato,[5] and Y. Kubozono[6]

[1]*Japan Advanced Institute of Science and Technology, Tatsunokuchi, Ishikawa 923-1292, Japan*

[2]*Institute for Materials Research, Tohoku University, Sendai, 980-8577, Japan*

[3]*CREST, Japan Science and Technology Corporation, Kawaguchi, 332-0012, Japan*

[4]*Department of Applied Physics, Nagoya University, Nagoya 464-8062, Japan*

[5]*Spring-8, Japan Synchrotron Radiation Research Institute, Hyogo 679-5198, Japan*

[6]*Institute for Molecular Science, Okazaki 444-8585, Japan*

(Received 22 October 2002; published 3 March 2003)

Rare-earth-metal-doped fullerides with nominal composition of R_3C_{70} (R=Sm, Eu) adopt a pseudomonoclinic structure in which C_{70} dimers glued with rare-earth ions are involved. High-pressure powder x-ray diffraction experiments revealed that these compounds undergo a reversible first-order structural phase transition at 1.5 GPa, associated with 2.7%–2.9% reduction of the unit cell volume. Structural analyses showed that the rare-earth ions, which are located close to the edge of tetrahedral sites at ambient pressure, move back to the center of the tetrahedral sites. Simultaneously, C_{70} molecules are realigned so that the fivefold (long) axes are perpendicular to the $(10\bar{1})$ or $(11\bar{1})_{fcc}$ plane at high pressure. The derived charge density map indicates that the transition is regarded as a structural change from dimers to three-dimensional polymers of fullerenes. These features are ascribed to the unique bonding nature in rare-earth C_{70} compounds.

DOI: 10.1103/PhysRevB.67.094101 PACS number(s): 61.48.+c, 61.10.Nz

INTRODUCTION

Intercalation of fullerites with metals has afforded a rich variety of materials, which have attracted considerable interest in this decade. Among them, intercalation compounds with rare-earth metals are much less known due to the difficulty in synthesis. Recently, researchers have have found several crystalline phases, including superconductors[1,2] and ferromagnetic compounds[3,4] in this family of materials.

From the structural point of view, four stable rare-earth-metal-fulleride phases $R_{2.75}C_{60}$ (R=Yb and Sm) (Refs. 1 and 2), R_6C_{60} (R=Sm and Eu) (Refs. 5 and 3), $R_{2.78}C_{70}$ (R=Sm) (Refs. 6 and 7), and R_9C_{70} (R=Eu) (Ref. 4) have been identified. In contrast to the saturation phases R_6C_{60} and R_9C_{70}, which have similar structures to those of the alkali-metal counterparts, the intermediate phases $Yb_{2.75}C_{60}$ and $Sm_{2.78}C_{70}$ are quite unique. In $R_{2.75}C_{60}$ compounds, tetrahedral vacancy ordering and the consequent shift of the cation position stabilize the intermediate concentration of rare-earth ions rather than the stoichiometric R_3C_{60}.[1,8] It is reported that alkaline-earth-metal-doped fulleride, $Ca_{2.75}C_{60}$, is another isostructural compound.[9] Tetrahedral vacancy is also encountered in $Sm_{2.78}C_{70}$, but it is not ordered in C_{70} compounds.[7] A very similar chemical composition determined by a Rietveld refinement indicates that the occurrence of tetrahedral vacancy sites is a generic property in nominal $R_{\sim 3}C_{60}$ and $R_{\sim 3}C_{70}$ systems.

A notable feature of $Sm_{2.78}C_{70}$ is that this structure consists of C_{70} dimers glued with rare-earth ions.[7] The Rietveld analysis has shown that the distance between Sm-C is considerably small, and a maximum entropy method (MEM) has revealed that there exists a strong electron density in between Sm and carbon, connecting two neighboring C_{70} molecules, via tetrahedral Sm ions. Figure 1 shows an equicontour map of electron density derived by the MEM-Rietveld analysis.[7] One of the tetrahedral anions with occupancy of nearly unity connects neighboring C_{70} molecules. Due to this dimerization, C_{70} molecules are orientationally ordered, as shown in Fig. 1.

In general, the interaction between intercalated alkali metals and fullerene moieties is known to be weak.[10] In the case of rare-earth metals, on the other hand, it has been pointed out that the bonding nature between C and metals is significantly different. In $Yb_{2.75}C_{60}$ (Ref. 1) the shortest Yb-C bond is 2.6–2.9 Å, which is slightly smaller than the sum of the ionic radius of Yb^{2+} and Van der Waals radius of carbon (1.71 Å). The Sm-C bond in $Sm_{2.78}C_{70}$ is expected to be much stronger than the Yb-C bonds in $Yb_{2.75}C_{60}$, since the observed Sm-C distance, 2.47(1) Å is markedly smaller than

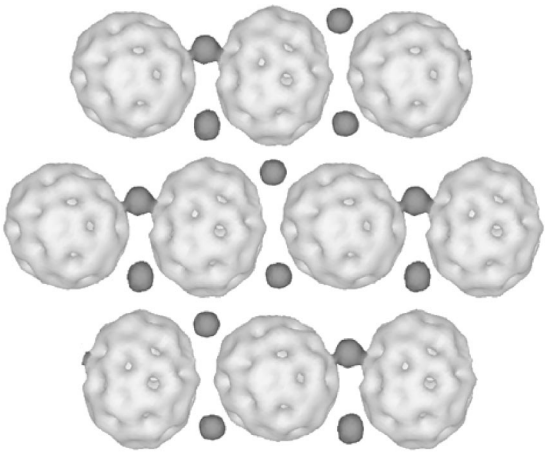

FIG. 1. Equicontour ($0.6e$ Å^{-3}) density map of the MEM charge density of $Sm_{2.78}C_{70}$ at ambient pressure, viewed from the $[111]_{fcc}$ direction.

the sum of the Sm^{2+} ionic radius 1.2 Å and carbon Van der Waals radius. In contrast to the well known interfullerene bonding via 2+2 cycloaddition and C-C single bonds,[11,12] the C_{70}-*M*-C_{70}-type bonding in solids is quite unique, possibly offering a new opportunity to investigate novel structural properties based on this interfullerene bonds. One of particular interest is the high-pressure effect, because it has provided numerous important and interesting information on the bonding properties in fullerites and fullerides.

In this paper, we report a synthesis of Eu_3C_{70} and Yb_3C_{70}, forming an isostructural series with Sm_3C_{70}, followed by investigation of the hydrostatic pressure effect on the structure of Sm_3C_{70} and Eu_3C_{70}. We found that these substances undergo first-order phase transitions at around 1.5 GPa, associated with a discontinuous volume reduction and a pressure hysteresis of 0.2 GPa. The Rietveld analysis of the high-pressure phase of Sm_3C_{70} indicates that the tetrahedral Sm^{2+} ions, which were located close to the edge of the site, move back to the site center in the high-pressure phase. The size of the tetrahedral site in the high-pressure phase is smaller than the ionic radii of Sm^{2+} and Eu^{2+}. These structural features at the high-pressure phase agree well with the a three-dimensional polymerlike charge density map, calculated by a combined method of the Rietveld analysis and MEM.[13]

EXPERIMENT

The compound with a nominal composition of R_3C_{70} has been synthesized by a solid-state reaction of stoichiometric mixture of metals and C_{70} powders. Mixed powders were sealed in quartz tubes under high vacuum of 2×10^{-6} torr. The tubes were annealed at 450 °C for 4 days and cooled down slowly to room temperature in a furnace. In a previous paper, we have reported the synthesis and crystal structure of Sm_3C_{70} (Refs. 6 and 7) and Eu_3C_{70} (Ref. 4), and showed that R_3C_{70} fullerides are very stable compounds. We have also succeeded in obtaining the Yb_3C_{70} fulleride by the same synthesis procedure.

For a fundamental characterization, high-resolution synchrotron x-ray powder diffraction data were recorded at room temperature on the beamline BL02B2 at the Super Photon Ring (SPring-8), Japan.[14] The samples of R_3C_{70} were sealed in thin glass capillaries of 0.3 mm in outer diameter for these experiments. In high-pressure experiments, quasihydrostatic pressure was generated by a diamond anvil cell (DAC), which was equipped with an inconel gasket. The diameter of the top face of the diamond culet was 1 mm, and the sample was introduced in a hole made in the gasket 0.2 mm in depth and 0.4 mm in diameter inside a controlled atmosphere of argon. Silicone oil was used as a pressure medium. Pressure was measured with the ruby-flourescence method. The high-pressure synchrotron x-ray diffraction experiments at ambient temperature were performed on beamline BL10XU at SPring-8. The diffraction patterns were collected using an image-plate detector with 5 min exposure time. Integration of the two-dimensional diffraction images was performed with a local PIP software. The valence states of rare-earth ions at high pressure have been inspected by the x-ray absorption near edge structure (XANES) spectra on the beamline BL01B1 at SPring-8. Rietveld refinement was made using GSAS software,[15] combined with MEM (Ref. 13) using the ENIGMA package.[16]

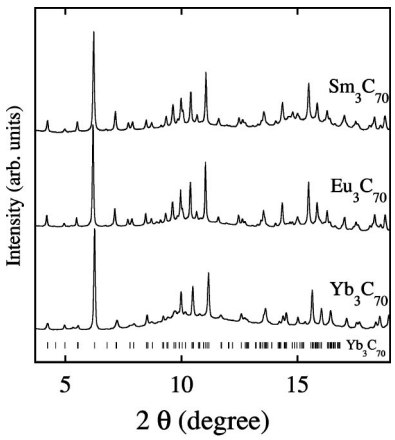

FIG. 2. Synchrotron x-ray powder diffraction profiles of nominal (a) Sm_3C_{70} (b) Eu_3C_{70} and (c) Yb_3C_{70}. Ticks mark positions of allowed reflections for Yb_3C_{70}.

RESULTS

Figure 2 shows the ambient pressure x-ray diffraction patterns of Sm_3C_{70}, Eu_3C_{70} and Yb_3C_{70}, recorded at $\lambda = 0.688\,83(1)$ Å. All of the diffraction patterns can be indexed on monoclinic cells with the lattice parameters summarized in Table I. The lattice parameter $a = 14.926(2)$ Å of Eu_3C_{70} is comparable to that of fcc structure of undoped C_{70}.[17] In a similar manner to Sm_3C_{70}, the unit cell of Eu_3C_{70} and Yb_3C_{70} is derived by a deformation of the fcc cell, in which intercalated metal ions occupy the tetrahedral and octahedral sites in a conventional way. Due to the similar diffraction profiles, Eu_3C_{70} and Yb_3C_{70} are expected to be isostructual to Sm_3C_{70}, in which C_{70} molecules are orientationally ordered and bridged by metal ions forming a dimer structure (Fig. 1). Details of the dimer structure have been described in our previous paper,[7] where the exact chemical representation of nominal Sm_3C_{70} phase was obtained as $Sm_{2.78}C_{70}$ due to the tetrahedral vacancy. The cell dimensions in Table I indicate that similar composition is also likely in Eu_3C_{70} and Yb_3C_{70}. However, we represent this phase as R_3C_{70} in this paper.

According to a geometrical consideration on the unit cell, it is expected that the volume of unit cell of R_3C_{70} is considerably smaller than that of K_3C_{70} (fcc, $a = 14.86$ Å),[18] because of the two reasons. First, the ionic radius of Sm^{2+} ($r \sim 1.2$ Å) is smaller than the ionic radius of K^+

TABLE I. Lattice parameters for R_3C_{70} (R = Sm, Eu, and Yb).

Materials	Lattice parameters
Sm_3C_{70}	$14.860(1)\times10.091(2)\times10.918(2)$ Å^3, $\beta = 96.173(5)°$
Eu_3C_{70}	$14.926(2)\times10.130(1)\times10.950(1)$ Å^3, $\beta = 96.111(5)°$
Yb_3C_{70}	$14.774(1)\times9.991(1)\times10.897(1)$ Å^3, $\beta = 96.072(5)°$

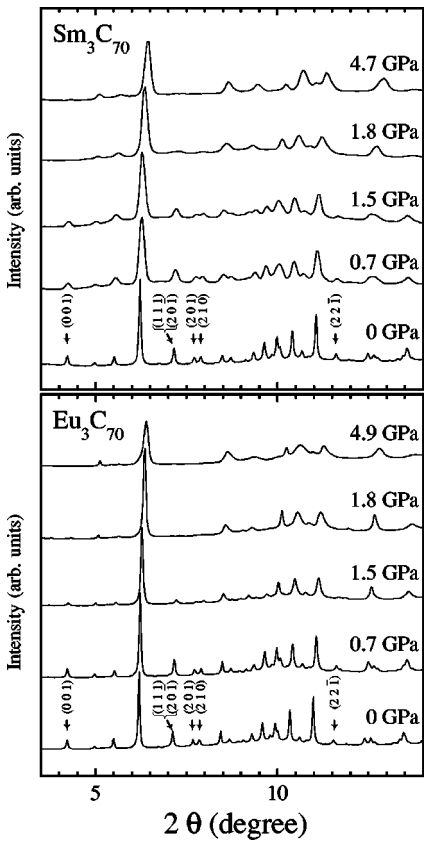

FIG. 3. Pressure evolution of the diffraction profiles of Sm_3C_{70} (top) and Eu_3C_{70} (bottom).

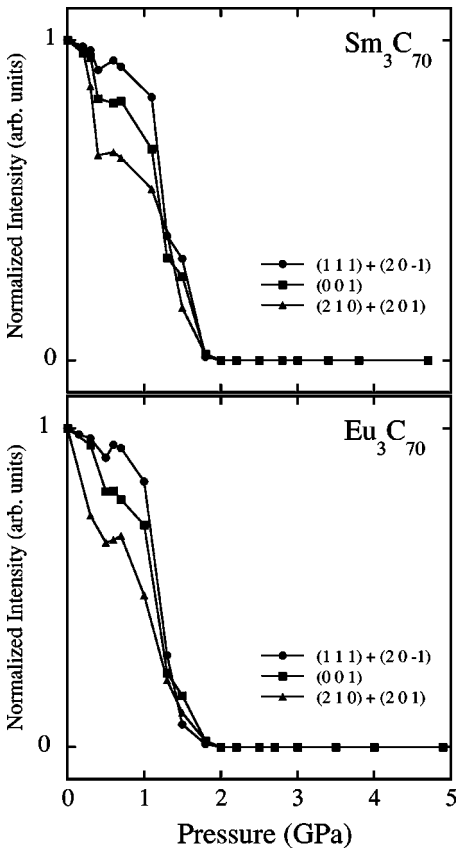

FIG. 4. Pressure variation of the normalized intesity of reflections (0 0 1), {(1 1 1), (2 0 $\bar{1}$)}, {(2 1 0), (2 0 1)} in diffraction profiles of Sm_3C_{70} and Eu_3C_{70}.

($r \sim 1.35$ Å). Second, enhanced Madelung energy in rare-earth fullerides induces further lattice contraction, because Sm, Eu, and Yb ions are divalent, while K is monovalent. However, the volume/C_{70} values of R_3C_{70} were found to be comparable to that of K_3C_{70} in contradiction to the above simple considration. The unexpectedly large volume/C_{70} in R_3C_{70} may indicate that the dimerization induces a significant realignment of C_{70} molecules and, consequently, rather loose packing.

In a zigzag alignment of ellipsoidal C_{70} molecules (Fig. 1), it is noted that the long (fivefold) axes of all C_{70} molecules are perpendicular to the *b* axis. In fact, the *b* parameter (=10.094 Å) is nearly identical to the C_{60}-C_{60} distance (10.02 Å) in undoped fcc C_{60}, in agreement with the C_{70} alignment perpendicular to the *b* axis. In the *ac* plane, on the other hand, significant expansion is observed in the $a(=14.862\ \text{Å} > \sqrt{2} \times b = 14.275\ \text{Å})$ and $c(=10.922\ \text{Å})$ parameters.

The formation of the dimer structure in Eu and Yb compounds is still an open question. However, we presume that similar dimer structure exists at least in Eu_3C_{70}, since the volume/C_{70} of this compound is even larger than that of K_3C_{70}. Additional evidence is provided from the high-pressure experiment, which showed an occurrence of identical phase transitions in Sm_3C_{70} and Eu_3C_{70}.

High-pressure x-ray powder diffraction profiles of Sm_3C_{70} and Eu_3C_{70} were collected at pressures between ambient and 5.0 GPa. Figure 3 shows the pressure evolution of the diffraction pattern of Sm_3C_{70} and Eu_3C_{70}. When a pressure of 1.3 GPa was reached, the diffraction patterns obviously showed weakening of a group of reflections (0 0 1), {(1 1 1), (2 0 $\bar{1}$)}, (2 1 0), and (2 0 1) (marked by arrows) for both cases of Sm_3C_{70} and Eu_3C_{70}. Figure 4 shows the pressure variation of the integrated intensity of reflections (0 0 1), {(1 1 1), (2 0 $\bar{1}$)}, {(2 1 0), (2 0 1)}, normalized by the ambient pressure values. The intensity of these peaks becomes negligible above 1.8 GPa, indicative of the occurrence of a phase transition.

Despite the peak broadening, the indexing process of the diffraction profiles at high pressure was successfully made on a monoclinic cell. The cell parameters extracted by the Le Bail fit at 1.8 GPa were $a=14.467(3)$ Å, $b=9.760(3)$ Å, $c=10.628(3)$ Å, $\beta=96.209(5)°$ and $a=14.533(3)$ Å, $b=9.826(3)$ Å, $c=10.700(2)$ Å, $\beta=96.216(5)°$ for Sm_3C_{70} and Eu_3C_{70}, respectively. These cell parameters are very similar to those at ambient pressure, indicating that the high-pressure structure is essentially similar to that at ambient pressure. A closer inspection of the space group at the high-pressure phase was made by the Rietveld analysis, which will be described in a following section.

To confirm the occurrence of the phase transition, we plot in Fig. 5 the pressure evolution of the cell parameters of Sm_3C_{70} and Eu_3C_{70} extracted by the Le Bail method. All the parameters display discontinuous changes at about 1.5 GPa.

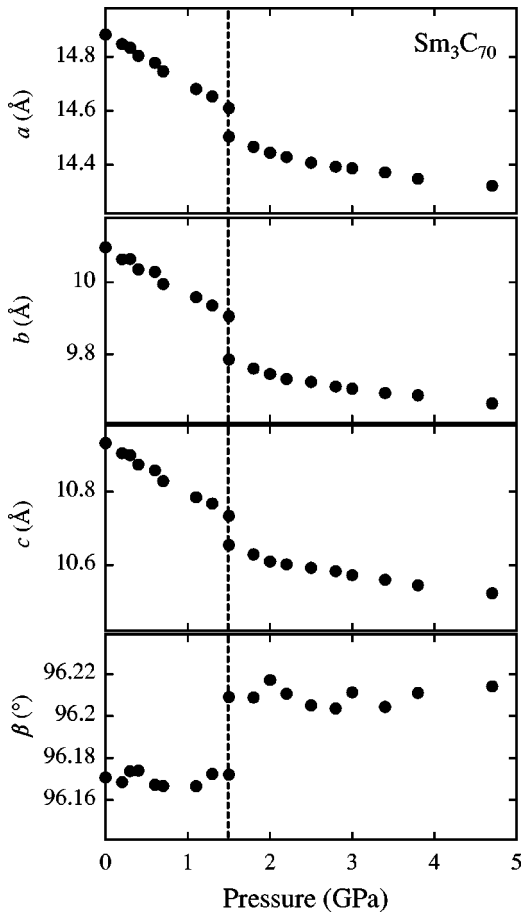

FIG. 5. Pressure dependence of the cell parameters *a*, *b*, *c*, and β (from top to bottom) for Sm_3C_{70} extracted by the Le Bail method. Open and solid circles represent points for the low- and high-pressure phases, respectively.

The diffraction patterns at 1.5 GPa showed a two-phase behavior both in Sm_3C_{70} and Eu_3C_{70}. In this case, the two-phase refinements converged smoothly, resulting in the two sets of lattice parameters $a=14.610(5)$ Å, $b=9.905(4)$ Å, $c=10.734(5)$ Å, $\beta=96.078(7)°$ and $a=14.504(5)$ Å, $b=9.785(5)$ Å, $c=10.654(5)$ Å, $\beta=96.209(7)°$ for Sm_3C_{70}. These two sets correspond to the low- and high-pressure phases, respectively, showing a volume reduction of 2.7%. A similar analysis on Eu_3C_{70} gave a 2.9% decrease in volume at the transition. The decompression experiments showed a slight hysteresis behavior of $P=0.2$ GPa for both Sm_3C_{70} and Eu_3C_{70}. All these results provide unambiguous evidence of the occurrence of a first-order phase transition at 1.5 GPa. Another implication from Fig. 5 is that the compression process is essentially isotropic within an experimental error. Since the covalent bond is limited within the dimer unit, the whole crystal is regarded as isotropic, in contrast to the anisotropic compression of polymeric fullerene structures.[19]

DISCUSSION: GEOMETRICAL CONSIDERATIONS

Figure 6 shows the pressure evolution of the unit cell volume of Sm_3C_{70} and Eu_3C_{70} obtained from the data in Fig. 5, together with the least-squares fit to the semiempirical second-order Murnaghan equation of states[20] (EOS):

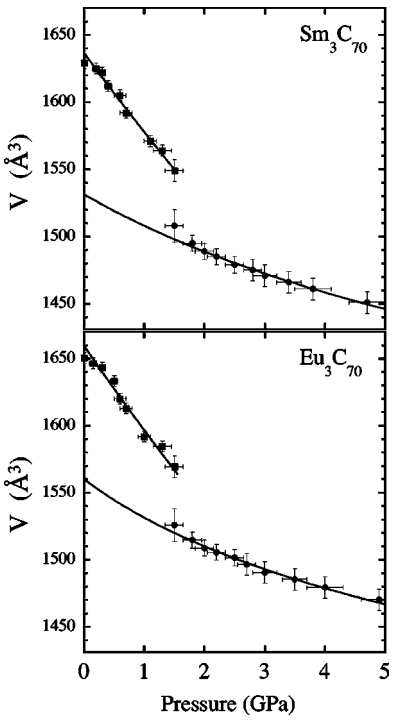

FIG. 6. Pressure dependence of the volume of pseudomonoclinic unit cell extracted by the Le-Bail method for Sm_3C_{70} (top) and Eu_3C_{70} (bottom). Solid lines show the least-squares fit to the second-order Murnaghan equation of states.

$$P=(K_0/K_0')[(V_0/V)^{K_0'}-1]$$

for both low- and high-pressure regions. K_0 is the atmospheric-pressure isothermal bulk modulus, K_0' is its pressure derivative ($=dK_0/dP$), and V_0 is the volume of the unit cell at zero pressure. For the low-pressure region, the fit results in values of $K_0=25.9(4)$ GPa, $K_0'=12.0(5)$ for Sm_3C_{70} and $K_0=25.4(4)$ GPa, $K_0'=16.9(5)$ for Eu_3C_{70}. The extracted values of the volume compressibility $\kappa=1/K_0$ at the low-pressure region are $\kappa=0.038(1)$ GPa^{-1} and 0.039(1) GPa^{-1} for Sm_3C_{70} and Eu_3C_{70}, respectively. These are comparable to those measured for the fcc fulleride phases, K_3C_{60} [0.036(3) GPa^{-1}] (Ref. 21) and Rb_3C_{60} (0.046(3) GPa^{-1}) (Refs. 21 and 22).

For the high-pressure phase, the extracted values of volume compressibility, $\kappa=0.020(1)$GPa^{-1} and 0.022(1) GPa^{-1} for Sm_3C_{70} and Eu_3C_{70}, respectively, are much smaller than those at the low-pressure phase, suggesting much more tight crystal packing or stronger interaction between dopant cations and fullerene anions at high-pressure. It is also noted that no evidence of anisotropy was found in the high pressure phase.

These experimental results allow us to postulate two hypotheses on the mechanism of the pressure-induced phase transition. One is the pressure-induced valence change from R^{2+} to R^{3+}, which indeed occurred in the SmS compound.[23] In the trivalent state, the enhanced Madelung energy might

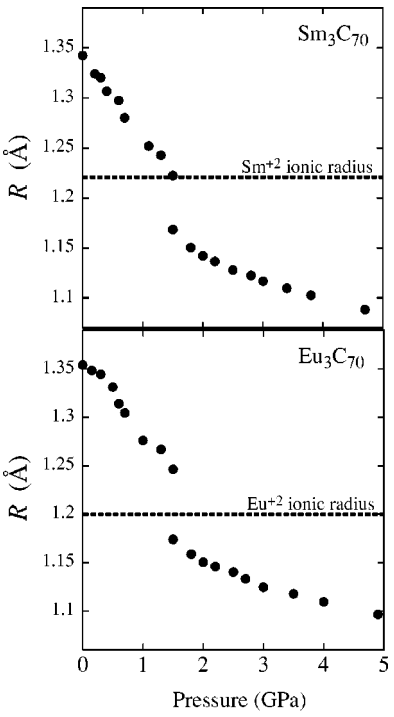

FIG. 7. Pressure dependence of average size of tetrahedral interstitial sites, which are geometrically calculated from the lattice parameters and average radius of C_{70} molecule assuming a spherical shape.

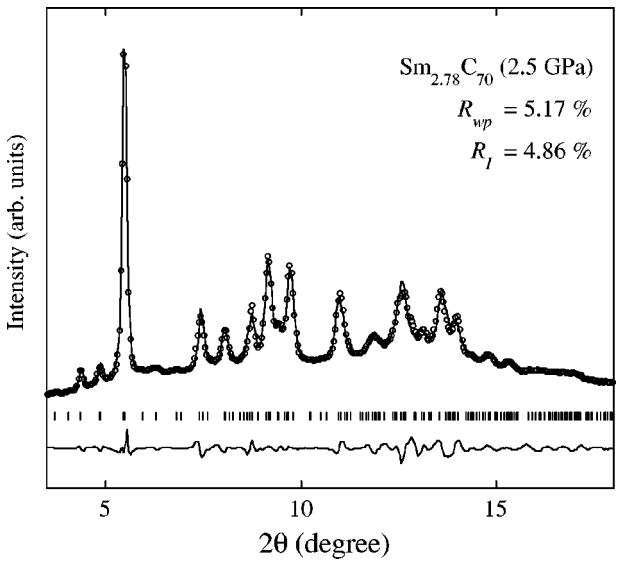

FIG. 8. Rietveld refinement on the x-ray diffraction pattern of $Sm_{2.78}C_{70}$ at 2.5 GPa, within a ellipsoidal C_{70} model. Top: the raw data (open circles) and the best-fit profile (solid line). Middle: peak positions. Bottom: the difference between the experimental and calculated patterns.

cause the shrinking and hardening of the cell. To test this hypothesis, we have measured XANES spectra of Sm ions in Sm_3C_{70} at high pressure. The high-pressure XANES spectra clearly showed that the average valence of Sm ion remains unchanged at 2+ well above the transition pressure 1.5 GPa. Therefore, we excluded the possibility of the valence change.

The second hypothesis is a purely structural origin. As discussed above, the crystal structure of R_3C_{70} at ambient pressure is a zigzag packing of metal-bridged dimers, forming a relatively large empty space in the interstices. Hence, the second possibility, which may be simple and convincing, is the collapsing of the dimer structure due to a steric crowding of dopant cations and fullerene anions at high pressure. For clarifying this hypothesis and understanding the mechanism of the structural transition, the interrelation between the size of interstitial sites and the ionic radii of intercalants would be an important key. Since the high-pressure XANES experiment confirmed that the Sm ion is divalent, the discussion related to the size of ionic radius should be based on the divalent ionic radius. Figure 7 shows the pressure dependence of the average size of the tetrahedral interstitial sites, which are geometrically calculated from the lattice parameters using the average radius of the spherical C_{70} molecule. At ambient pressure, the size of tetrahedral interstitial site is larger than the divalent ionic radius of the intercalant for both Sm_3C_{70} and Eu_3C_{70}, indicating no steric crowding for metal ions. Metal ions are stabilized at off-centered positions both in octahedral and tetrahedral sites. At high pressure, the structural phase transition causes a large volume decrease of the unit cell and thus a size decrease of the interstitial sites. Particularly, the size of the tetrahedral interstitial site is reduced just to fit to the size of the metal ions (Fig. 7). The smaller compressibility at the high-pressure phase is attributable to the steric crowding.

DISCUSSION: MEM-RIETVELD ANALYSIS

For further understanding the nature of the phase transition, we have made a MEM-Rietveld analysis.[13] The first Rietveld refinement of the high-pressure phase at 2.5GPa for Sm_3C_{60} was done with the spherical shell model, where C_{70} molecules are approximated by two sherical shells of charge, representing the long and short axes of C_{70}. Despite the simpleness of the model, the obtained locations of the metal ions are known to be reliable since the electron densities of the rare-earth ions are large enough comparing to that of carbon atoms. This refinement started from the structural model at ambient pressure, where metal ions in tetrahedral and octahedral interstitial sites are placed at the same position and with the same occupancy to those in the ambient-pressure structure.[7] Since we have only 36 resolved peaks with 196 reflections involved, due to the peak broadening, we needed to reduce the number of refined parameters. Thus we fixed the occupancies of Sm ions at the ambient-pressure values and refined 29 parameters, including positions and thermal parameters of Sm ions, a thermal parameter of carbon, and diameters of two spherical shells. The fixed occupancy is a reasonable assumption, since all experiments were carried out at room temperature, where migration of intercalated Sm ions is not activated.

In the primary refinement with $R_I < 10\%$, the tetrahedral Sm ions were found to be situated at $(\sim\frac{1}{4},\sim\frac{1}{2},0)$, $(\sim\frac{3}{4},\sim\frac{1}{2},0)$, $(\sim\frac{1}{4},0,\sim\frac{1}{2})$, and $(\sim\frac{3}{4},0,\sim\frac{1}{2})$, namely, close to the center of the tetrahedral sites in the deformed fcc structure.

TABLE II. Structural parameters for $Sm_{2.78}C_{70}$ at 2.5 GPa. Here, we use Cartesian coordinates expressed in angstroms. The **y** axis of the coordinate system is along the monoclinic *b*, axis the **z** axis along the *a* axis, and $\mathbf{x}=\mathbf{y}\times\mathbf{z}$. The the long axis of the ellipsoidal shell model of C_{70} is directed parallel to the *a* axis, the center of the shell is placed at (0,0,0), and the shell is subjected to the rotations

$$\begin{pmatrix} \cos\psi & \sin\psi & 0 \\ -\sin\psi & \cos\psi & 0 \\ 0 & 0 & 1 \end{pmatrix} \begin{pmatrix} \cos\theta & 0 & \sin\theta \\ 0 & 1 & 0 \\ -\sin\theta & 0 & \cos\theta \end{pmatrix} \begin{pmatrix} \cos\phi & \sin\phi & 0 \\ -\sin\phi & \cos\phi & 0 \\ 0 & 0 & 1 \end{pmatrix}.$$

$Sm_{2.78}C_{70}$	High-pressure phase (2.5 GPa)
Lattice parameter	$14.408(2)\times 9.723(2)\times 10.592(2)$ Å^3, $\beta=96.205(5)°$
Space group	$P1$
Rietveld fit	$R_{wp}=5.17\%$, $R_I=4.86\%$, $\chi^2=7.32$
Center of the rigid C_{70} and Eulerian angles	$C_{70}(1)$ 0.0 0.0 0.0 $\psi=54°$ $\theta=0°$ $\phi=0°$
	$C_{70}(2)$ 0.5 0.5 0.5 $\psi=54°$ $\theta=0°$ $\phi=0°$
Atomic coordinates and occupancies	Sm(1) 0.250(7) 0.977(7) 0.517(8) 1.00
	Sm(2) 0.743(8) 0.013(6) 0.477(7) 0.93
	Sm(3) 0.231(8) 0.489(8) 0.970(8) 0.68
	Sm(4) 0.747(7) 0.531(6) 0.020(6) 0.95
	Sm(5) 0.011(7) 0.431(6) 0.455(7) 0.50
	Sm(6) 0.988(6) 0.429(8) 0.460(8) 0.50
	Sm(7) 0.510(8) 0.914(8) 0.041(6) 0.50
	Sm(8) 0.489(7) 0.920(7) 0.039(8) 0.50
Thermal parameters	$B(Sm_{1,2,3,4})=0.03(1)$ Å^2
	$B(Sm_{5,6,7,8})=0.80(2)$ Å^2
	$B(C)=0.08(2)$ Å^2

The disappearance of the several diffraction peaks indexed as (0 0 1), (1 1 1), (2 0 $\overline{1}$), (2 1 0), and (2 0 1) is well accounted for by the shift of the tetrahedral Sm ions to the positions close to the high-symmetry points. However, experimental data indicate that these reflections are not exactly forbidden. In fact, the calculated structure factors of these reflections are finite, but about three orders of magnitude smaller than the main reflection $\{(200),(011)\}$. The result of the first Rietveld fit for the 2.5GPa data with the spherical shell model gave reliability factors of $R_{wp}=6.25\%$, $R_I=6.18\%$.

As for the space group of the high-pressure structure, the peak indexing and Le Bail processes implied that there are only three possible space groups $P1$, $P2$, and $P2/m$. We have inspected these three space groups in the first Rietveld process the reliability factor R_{wp} for $P2/m$ with 12 fitting parameters was always larger than 10%. The refinement with $P2$ space group and 16 fitting parameters gave R_{wp} of 8.72% and 8.53% for the spherical and ellipsoidal shell models, respectively. These values are considerably larger than $R_{wp}=6.25\%$ for the $P1$ space group and the spherical shell model. Hence, we concluded that the space group of the high-pressure phase is $P1$, which is identical to that at ambient pressure.[7] Since the Rietveld refinement itself showed that all the tetrahedral Sm is moved close to the high-symmetry points, this result is a bit puzzling. We presume that the low symmetry of the high-pressure phase is caused by the small occupancy of one particular tetrahedral site Sm(3), which does not allow higher symmetry.

In the second step of the analysis, we have computed charge density map with MEM using the structure factors obtained from the first Rietveld refinement with the spherical shell model. It is now well established that the imaging ability of the MEM-Rietveld analysis provides more detailed structural models beyond the initial model for the first Rietveld refinement.[13] In fact, the method has been successfully applied to structural determinations of endohedral metallofullerenes[24] and many other examples. Details of the method are described elsewhere.[13] To our surprise, the calulated MEM charge density predicted that the orientation of the long axis of all C_{70} molecules is perpendicular to the $(10\overline{1})$ or $(11\overline{1})_{fcc}$ plane.

Based upon the MEM's predition of the orientation of C_{70}, the second Rietveld refinement was carried out using an ellipsoidal shell model of C_{70} with fixed long and short axes of 7.9 Å and 7.1 Å, respectively. Since two of the fitting parameters—the diameters of two spheroids in the spherical shell model—are replaced by two orienation angles of the C_{70} ellipsoid in the ellipsoidal shell model, the total number of parameters remained 29. Figure 8 displays the x-ray diffraction pattern of the Sm_3C_{70} sample at 2.5 GPa with the result of the second Rietveld fit shown as a solid line. The result of this alaysis is summarized in Table II. The reliability

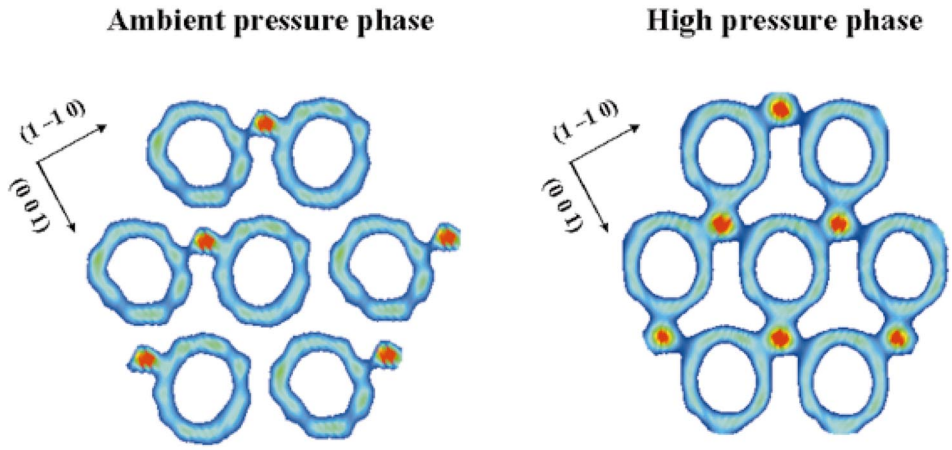

FIG. 9. (Color) Color contour map (from 0.6e Å to 5e Å^{-3}) of the cross section of the MEM charge density for $Sm_{2.78}C_{70}$ at ambient pressure (left) and at 2.5GPa (high-pressure phase) (right). The section was obtained by cutting the three-dimensional charge density map by the plane involving C-Sm(4)-C bonds, which is parallel to the (110) or $(111)_{fcc}$ plane.

factor of the second Rietveld analysis was R_{wp}= 5.17%, R_I= 4.86%, which is a significant improvement from the spherical shell model, considering that the number of refined parameters in the ellipsoidal shell model is identical to that in the spherical shell model. We also calculated the second MEM charge density based on the second Rietveld result. This MEM picture, however, presented no additional implication of more detailed structures. For a further refinement process, more fitting parameters are required. Considering the broadness of the diffraction pattern and limited number of resolved peaks, we stopped the analysis to avoid overinterpretation. The second (final) MEM charge density is shown in Fig. 9, combined with that at ambient pressure.

The final result of the Rietveld refinement does not seriously affect the location of Sm ions determined in the first refinement within a spherical shell model. In contrast to the tetrahedral site, occupied by a single Sm^{2+} ion, there still exist two stable positions for Sm^{2+} ions in the octahedral site, though these two positions are much closer to each other than at ambient pressure. These two sites are randomly occupied by Sm ions in a mutually exclusive way, removing unphysically short contacts.

Combining the MEM-Rietveld structural analysis of the high-pressure phase with the consideration of the size of the tetrahedral interstitial site (Fig. 7), the transition can be explained by the simultaneous movement of rare-earth ions and C_{70} molecules, due to the steric crowding of dopant cations and fullerene anions under high pressure. At the ambient-pressure phase, the tetrahedral ions are shifted from the site center since they participate the formation of rare-earth–carbon bonds. By application of hydrostatic pressure, the metal ions are naturally pressed back to the site center due to external force, possibly causing a collapse of the dimer structure and a reorientation of C_{70}. Figure 10 shows a schematic illustration of the high-pressure structure. The long axis of all C_{70} molecules is aligned perpendicular to $(10\bar{1})$ or $(11\bar{1})_{fcc}$

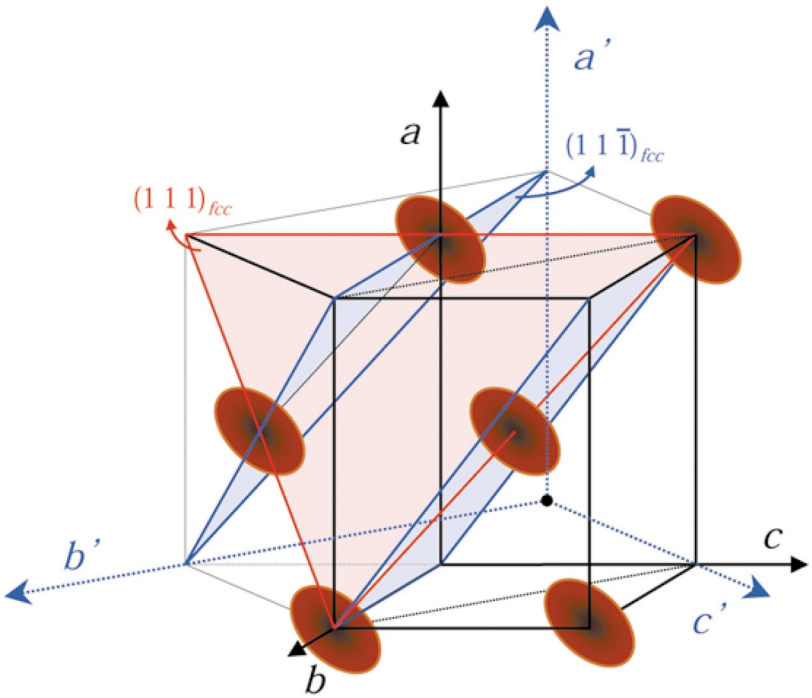

FIG. 10. (Color) Schematic illustration of the pseudomonoclinic and parent fcc cells. Directions of unit vectors for the former and latter cells are represented by black solid and blue dotted lines, respectively. The MEM charge density map in Fig. 9 is drawn for the pink-colored (110) or $(111)_{fcc}$ plane. At the high-pressure phase, the long axis of all C_{70} molecules (brown ellipsoids) is perpendicular to the $(10\bar{1})$ or $(11\bar{1})_{fcc}$ plane hatched with light blue color.

plane (hatched in ligh blue), forming a closely packed distorted rhombohedral structure.

These changes are well described by the MEM charge density map for ambient and high pressure shown in Fig. 9, which is a cross section cut by a plane parallel to (110) or $(111)_{fcc}$. A new indication from this figure is that strong hybridization between rare-earth metals and fullerene cages is established. This state is not surprising when one recalls that the size of the tetrahedral holes is smaller than the ionic radius of Sm^{2+} in the high-pressure phase as shown in Fig. 7. This state might be regarded as a new type of polymeric fullerene structure with a three-dimensional network. The small compressibility of the high-pressure phase, which is only half of that for the low-pressure phase (Fig. 6), is also reasonably understood from Fig. 9. Taking the comparable compressibility of the low-pressure phase to that of alkali-metal fullerides K_3C_{60} or Rb_3C_{60} into account, the interaction in the high-pressure phase of Sm_3C_{70} is much stronger than the typical ionic fullerides.

In the present MEM-Rietveld analysis, we were not able to determine the orientational state around the long axis of the C_{70} molecule, due to the broadening of diffraction pattern at high pressure. There remain two possble orientational states: One scenario is that the orientation is really disordered, and the other is that the orientaion is ordered but the available data are not sufficient for a full determination. For the latter case, a distorted rhombohedral structure necessiates nearly threefold symmetry in the C_{70} molecule, which is absent. Thus, if this is the case, the neighboring C_{70}'s are not identical to each other. For a full understanding of the high-pressure structure, the improvement of diffraction pattern at high pressure is crucial. For instance, use of a gas pressure medium such as helium will be promising.

CONCLUSIONS

In conclusion, we have synthesized a stable isostructural series of rare-earth-metal fullerides R_3C_{70} (R=Yb, Eu, and Sm). These compounds adopt a pseudomonoclinic structure, which is derived by a deformation of the well-known fcc structure. In analogy to the fully analyzed compound $Sm_{2.78}C_{70}$ we suggest that the sructure involves a C_{70}-R-C_{70} dimer unit. A high pressure x-ray diffraction experiment revealed that Sm_3C_{70} and Eu_3C_{70} compounds undergo a reversible first-order structural phase transition at about 1.5 GPa. This transition is accompanied by a discontinuous volume reduction of 2.7%–2.9%. The MEM-Rietveld analysis within the ellipsoidal shell model of C_{70} showed that rare-earth ions, which occupied an off-centered position of tetrahedral interstitial sites at ambient pressure, were pushed back close to the center of the tetrahedral site in the high-pressure phase. Simultaneously, C_{70} molecules were reorientated so that the long axis is aligned perpendicular to the $(10\bar{1})$ or $(11\bar{1})_{fcc}$ plane. The MEM charge density map has shown a three-dimensional polymerlike bonding network which agrees quite well with the small compressibility for the high-pressure phase. The present results clearly demonstrate that the unique bonding nature of rare-earth-metal intercalated fullerides brings about a new structural aspect of fullerides, which is related to the orientation of fullerene molecules.

ACKNOWLEDGMENTS

This work has been partly supported by a grant from the Ministry of Education, Sport, Science, and Culture, Japan (Grant No. 13440110). We thank O. Shimomura and A. Fujiwara for stimulating discussions. D.H.C. thanks International Communication Foundation and the Rotary Yoneyama Foundation for their financial support.

[1] E. Ozdas, A. R. Kortan, N. Kopylov, A. P. Ramirez, T. Siegrist, K. M. Rabe, H. E. Bair, S. Schuppler, and P. H. Citrin, Nature (London) **375**, 126 (1995).

[2] X. H. Chen and G. Roth, Phys. Rev. B **52**, 15 534 (1995).

[3] K. Ishii, A. Fujiwara, H. Suematsu, and Y. Kubozono, Phys. Rev. B **65**, 134431 (2002).

[4] T. Takenobu, H. C. Dam, S. Margadona, K. Prassides, Y. Kubzono, A. N. Fitch, and Y. Iwasa, J. Am. Chem. Soc. **125**, 1897 (2003).

[5] X. H. Chen, Z. S. Liu, S. Y. Li, H. C. Dam, and Y. Iwasa, Phys. Rev. B **60**, 6183 (1999).

[6] X. H. Chen, H. C. Dam, Z. Sun, T. Takenobu, Z. S. Liu, and Y. Iwasa, J. Am. Chem. Soc. **122**, 5729 (2000).

[7] H. C. Dam, Y. Iwasa, X. H. Chen, T. Takenobu, T. Ito, T. Mtani, E. Nishibori, M. Takata, M. Sakata, and Y. Kubozono, Chem. Phys. Lett. **359**, 177 (2002).

[8] P. H. Citrin, E. Ozdas, S. Schuppler, A. R. Kortan, and K. B. Lyons, Phys. Rev. B **56**, 5213 (1997).

[9] E. Ozdas, A. R. Kortan, N. Kopylov, A. P. Ramirez, T. Siegrist, and P. H. Citrin (unpublished).

[10] M. Takata, N. Machida, E. Nishibori, B. Umeda, M. Sakata, K. Tanigaki, M. Kosaka, I. Hirosawa, and J. Mizuki, Jpn. J. Appl. Phys., Part 1 **38**, 122 (1999).

[11] P. W. Stephens, G. Bortel, G. Faigel, M. Tegze, A. Janossy, S. Pekker, G. Oszlanyi, and L. Forro, Nature (London) **370**, 636 (1994); G. Oszlanyi, G. Bortel, G. Faigel, L. Granasy, G. M. Bendele, P. W. Stephens, and L. Forro, Phys. Rev. B **54**, 11 849 (1996); G. M. Bedele, P. W. Stephens, K. Prassides, K. Vavekis, K. Kordatos, and K. Tanigaki, Phys. Rev. Lett. **80**, 736 (1998).

[12] Y. Iwasa, T. Arima, R. M. Fleming, T. Siegrist, O. Zhou, R. C. Haddon, L. J. Rothberg, K. B. Lyons, H. L. Carter, Jr., A. F. Hebard, R. Tycko, G. Dabbagh, J. J. Krajewski, G. A. Thomas, and T. Yagi, Science **264**, 1570 (1994); M. Nunez-Regueiro, L. Marques, J. -L. Hodeau, O. Bethoux, and P. Perroux, Phys. Rev. Lett. **74**, 278 (1995).

[13] M. Takata, E. Nishibori, and M. Sakata, Z. Kristallogr. **216**, 71 (2001).

[14] E. Nishibori, M. Takata, K. Kato, M. Sakata, Y. Kubota, S. Aoyagi, Y. Kuroiwa, M. Yamakata, and N. Ikeda, Nucl. Instrum. Methods Phys. Res. A **467-468**, 1045 (2001).

[15] A. C. Larson and R. B. von Dreele (unpublished).

[16] H. Tanaka, M. Takata, E. Nishibori, K. Kato, T. Iishi, and M. Sakata, Acta Crystallogr., Sect. B: Struct. Sci. **35**, 282 (2002).

[17] G. B. Vaughan, P. A. Heiney, J. E. Fischer, D. E. Luzzi, D. A. Ricketts-Foot, A. R. McGhie, Y. W. Hui, A. L. Smith, D. E. Cox, W. J. Romanow, B. H. Allen, N. Coustel, J. P. McCauley, and A. B. Smith, Science **254**, 1350 (1991).
[18] M. Kobayashi, Y. Akahama, H. Kawamura, H. Shinohara, H. Sato, and Y. Saito, Phys. Rev. B **48**, 16 877 (1993).
[19] S. Margadona, C. M. Brown, A. Lappas, K. Prassides, K. Tanigaki, K. D. Knudsen, T. L. Bihan, and M. Mezouar, Solid State Chem. **145**, 471 (1999).
[20] F. D. Murnaghan, Proc. Natl. Acad. Sci. U.S.A. **30**, 244 (1947); J. R. Macdonald and D. R. J. Powell, J. Res. Natl. Bur. Stand. Sect. A **75**, 441 (1971).
[21] O. Zhou, G. B. M. Vaughan, Q. Zhu, J. E. Fischer, P. A. Heiney, N. Coustel, J. P. McCauley, and A. B. Smith, Science **255**, 833 (1992).
[22] J. Diederichs, J. S. Schilling, K. W. Herwig, and W. B. Yelon, J. Phys. Chem. Solids **58**, 123 (1997).
[23] A. Chatterjee and A. K. Singh, Phys. Rev. B **6**, 2285 (1972).
[24] M. Takata, B. Umeda, E. Nishibori, M. Sakata, Y. Saito, M. Ohno, and H. Shinohara, Nature (London) **377**, 46 (1995).